Magn Reson Med Sci 2021; 20; 182–189
doi:10.2463/mrms.mp.2019-0180
Published Online: June 26, 2020

MAJOR PAPER

Three-dimensional Gradient-echo is Effective in Suppressing Radiofrequency Shielding by a Titanium Mesh

Yasuo Takatsu[1,2*], Rei Yoshida[3], Kenichiro Yamamura[4], Yuya Yamatani[5], Tsuyoshi Ueyama[6], Tetsuya Kimura[7], Yuriko Nohara[8], Tomohiro Sahara[9], Kengo Nishiyama[10], and Tosiaki Miyati[2]

Purpose: To determine which sequence for frequently used general contrast-enhanced brain MRI shows the least radiofrequency shielding effect of a titanium mesh in cranioplasty using a phantom.

Methods: A 1.5T MRI scanner was used. Frequently used general 2D and 3D spin-echo sequences (SE) and T_1 spoiled gradient echo sequences (GRE) used for MRI in clinical settings were adopted in this study. A titanium mesh was placed above a cubic phantom containing manganese chloride tetrahydrate and sodium chloride. The signal attenuation ratio and normalized absolute average deviation (NAAD) were calculated. Moreover, the flip angle (FA) dependency in SE and area of excitation dependency in 3D sequences were analyzed using NAAD.

Results: The signal attenuation ratio at the position nearest to the titanium mesh for 2D SE was 71.8% larger than that at the position nearest to the titanium mesh for 3D GRE. With regard to NAAD, 3D GRE showed the highest values among the sequences. When FA was increased, radiofrequency shielding effect was improved. There were no significant differences between the narrow and wide area of excitation. 3D GRE showed the least radiofrequency shielding effect, and it was considered as the optimal sequence for MRI in the presence of a titanium mesh.

Conclusion: 3D GRE shows the least radiofrequency shielding effect of a titanium mesh after cranioplasty among frequently used general sequences for contrast-enhanced brain MRI.

Keywords: *magnetic resonance imaging, radiofrequency-shielding effect, signal attenuation ratio, titanium mesh, pulse sequence*

Introduction

One of the most commonly used materials for cranioplasty is a titanium mesh owing to its excellent biocompatibility and mechanical performance.[1–5] In addition, studies have reported that titanium has non-ferromagnetic properties; therefore, it does not induce notable artifacts on MRI.[5]

However, a titanium mesh has been reported to cause radiofrequency (RF) shielding.[6] When time-varying RF waves are produced, electrical currents are induced in a metallic implant according to Faraday's law of induction.[7,8] With so-called eddy currents, the amplitude of the transmitted RF field can be reduced, i.e., the excitation flip angle (FA) can be reduced, and the signals inside the metallic implant can be shielded and reduced.[9]

In a B_1 map, the FA under a titanium mesh was shown to decrease visibly.[6] When RF shielding occurs, the actual FA in the tissue is lower than the nominal FA value entered by the operator.[9] Moreover, in similar situations, a report on vascular stents indicated that a decrease in signal intensity could be induced by eddy currents owing to a reduction in the amplitude of the transmitted RF field, thereby potentially shielding the signals.[9] When gradient echo sequence was used, the RF shielding decreased by a high FA.[8,10]

[1]Department of Radiological Technology, Faculty of Health and Welfare, Tokushima Bunri University, Kagawa, Japan
[2]Division of Health Sciences, Graduate School of Medical Sciences, Kanazawa University, Ishikawa, Japan
[3]Department of Radiology, Kurihara Central Hospital, Miyagi, Japan
[4]Department of Radiology, Osaka Medical College Hospital, Osaka, Japan
[5]Division of Central Radiology, Nara Medical University Hospital, Nara, Japan
[6]Department of Radiology, The University of Tokyo Hospital, Tokyo, Japan
[7]Department of Radiological Technology, Sakai City Medical Center, Osaka, Japan
[8]Department of Radiology, Daini Osaka Police Hospital, Osaka, Japan
[9]Division of Radiological Technology, Osaka City University Hospital, Osaka, Japan
[10]Department of Radiology, Osaka Red Cross Hospital, Osaka, Japan

[*]Corresponding author: Department of Radiological Technology, Faculty of Health and Welfare, Tokushima Bunri University, 1314-1, Shido, Sanuki, Kagawa 769-2193, Japan. Phone: +81-87-899-7293, E-mail: pcblue2@yahoo.co.jp

Received: December 3, 2019 | Accepted: April 24, 2020

After surgery for brain tumors, T_1-weighted imaging (T_1WI) with contrast medium is performed to assess the presence of remnant tumors and recurrence.[11] However, the influence of the RF shielding effect with the use of a titanium mesh is a concern. If the RF shielding effect is reduced using suitable sequences, high-quality images will be obtained.

With regard to sequence parameters, it has been reported that not only conventional two-dimensional (2D) spin echo (SE) but also fast SE (FSE),[12] three-dimensional (3D) gradient echo (GRE),[13–16] and 3D FSE[17,18] in T_1WI can be used for the assessment of brain tumors.

To date, it has not been reported whether the RF shielding effect with the use of a titanium mesh in cranioplasty is influenced by the above mentioned four frequently used general sequences for brain MRI. The present study aims to determine which sequence for the frequently used general contrast-enhanced brain MRI exhibits the least RF shielding effect of the titanium mesh after cranioplasty, using a phantom.

Materials and Methods

Ethical consideration

This study was approved by the Ethics Committee of Osaka Red Cross Hospital and performed using the opt-out method of the hospital website.

Scan conditions

A 1.5T MRI scanner (Achieva; Philips, Best, The Netherlands) with a quadrature head coil was used for imaging. A cubic bottle filled with 33 mg/L of manganese chloride tetrahydrate and 3.6 g/L of sodium chloride was used as a phantom (T_1 relaxation time, 726.7 ms; T_2 relaxation time, 92.6 ms) to mimic the human brain. The phantom was placed at the center of the coil, and a titanium mesh board (100 × 100 × 0.8 mm; hole diameter, 1.6 mm; hole interval, 3 mm; thickness, 0.8 mm), which is identical to the material used during actual cranioplasty, was placed on the phantom (Fig. 1a).

Sequence parameters for frequently used general sequences in clinical situations were used as follows: T_1-weighted brain MRI with contrast enhancement; 2D SE, 2D turbo SE (TSE; as FSE), volume isotropic TSE acquisition (VISTA) as 3D TSE, and 3D spoiled GRE in T_1WI is represented by T_1-fast-field echo (T_1-FFE) (Table 1). In VISTA, the variable FAs refocusing RF pulses are referred to as "refocusing controls." The smallest slice that can be set was used to eliminate the influence of the number of slices.

The same receiver bandwidths were set for the sequences, and the sequences were compared. The axial view was scanned at the center of the titanium mesh board. The scans were acquired six times.

Comparison among four T_1-weighted sequences

We assessed the differences in the sequences used in clinical examinations and identified the optimal imaging method for inspection with a titanium mesh after cranioplasty. Four sequences in clinical situations (Table 1) were compared.

Signal attenuation ratio

The signal attenuation ratio was calculated as the signal intensity of the image obtained in the presence of the

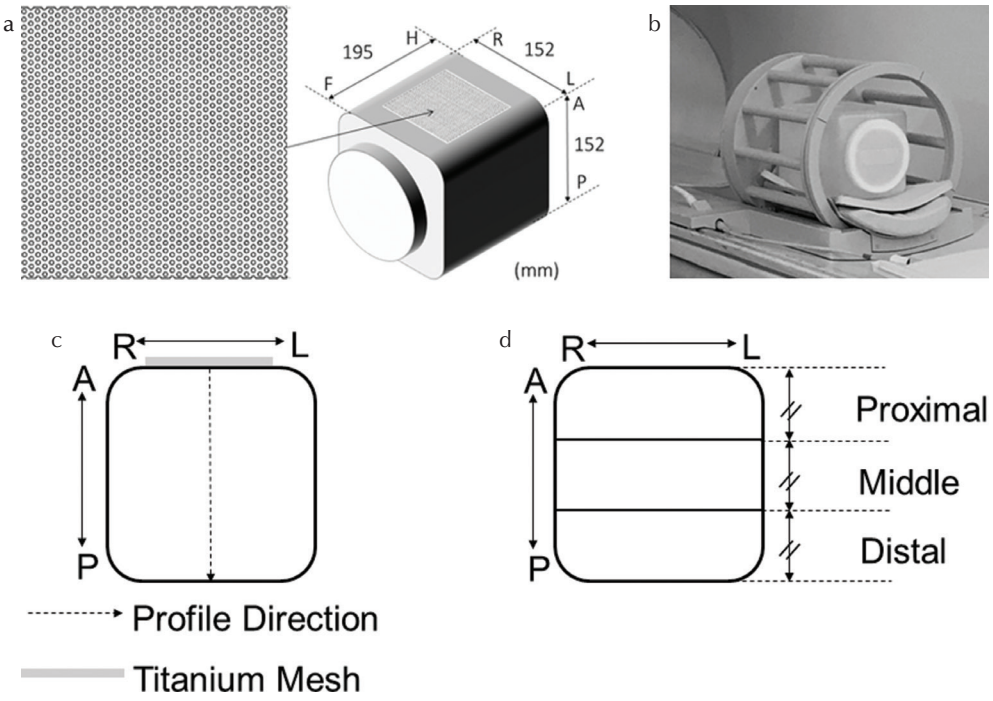

Fig. 1 (**a**) The titanium mesh and the cubic phantom. Phantom axis for the analysis. (**b**) Placement of the phantom in the coil. (**c**) Profile direction and position of the titanium mesh. The axial view is scanned at the center of the titanium mesh. Profiles for the signal attenuation ratio are created from the edge of the phantom at the proximal end of the titanium mesh to the edge of the opposite side of the phantom at right angles to the center of the titanium mesh. (**d**) Calculation for NAAD. The phantom-only image is divided into the following three sections: proximal, area under the titanium mesh; middle, center of the phantom image; distal, area far from the titanium mesh (50 × 150 mm^2 for each area). A, anterior direction; F, foot direction; H, head direction; L, left side; NAAD, normalized absolute average deviation; P, posterior direction; R, right side.

Table 1 Sequence parameters for routine T_1-weighted brain MRI with contrast enhancement

	TR (ms)	TE (ms)	FA (°)	TSE factor	Refocusing (control) (°)	Matrix (P × R)	FOV (mm)	3D non-selective	BW (Hz/pixel)	NSA	Slice	Slice thickness (mm)
2D SE	500	10	90	–	180	256 × 256	256 × 256	–	422.3	1	1	5
2D TSE	500	10 (eff.)	90	3	180	256 × 256	256 × 256	–	422.3	1	1	5
3D TSE (VISTA)	500	13 (eff.)	90	20	Yes (50)	256 × 256	256 × 256	Yes	422.3	1	3	5
3D T_1-FFE	25	4.2	30	–	–	256 × 256	256 × 256	–	422.3	1	3	5

BW, band width; eff., effective; FA, flip angle; FFE, fast field echo; NSA, number of signal averaged; P, phase encode direction; R, read out encode direction; SE, spin echo; TSE, turbo spin echo; VISTA, volume isotropic TSE acquisition.

titanium mesh divided by the signal intensity obtained in the absence of the mesh on assessing these images directly using ImageJ (Version 1.52a; National Institute of Health, Bethesda, MD, USA). If the signal intensity did not change, the signal attenuation ratio was 1.[6] The position of the phantom in the two cases—presence and absence of the titanium mesh—was the same (Fig. 1a and 1b).

To assess the effect of the board, profiles for the signal attenuation ratio were created at right angles to the center of the titanium mesh, i.e., from the edge of the phantom on the proximal end of the titanium mesh to the edge of the opposite side of the phantom (Fig. 1c).[6] The data of six scans were averaged. Imaging calculations were performed using ImageJ.

Normalized absolute average deviation

To evaluate uniformity as RF shielding dependency, normalized absolute average deviation (NAAD) was used.[19] NAAD was calculated using the following equation:

$$\mathrm{NAAD} = 100 \times \left[1 - \frac{1}{N\overline{Y}} \sum_{i=1}^{N} \left(\left| Y_i - \overline{Y} \right| \right) \right]$$

where Y_i is the individual pixel value within the measurement region of interest (MROI), $\overline{Y}$ is the mean of all pixels within the MROI, $|Y_i - \overline{Y}|$ is the absolute deviation for pixel i, and N is the total number of pixels within the MROI.[19]

The signal attenuation is influenced by the RF shielding effect in the periphery of the phantom under the titanium mesh. Therefore, if the ROI is placed in the phantom image, the signal attenuation area might not be appropriately assessed. To assess the NAAD of the entire phantom image, we used the mask method.[20] Mask images were created from images without the titanium mesh using discriminant analysis according to the Otsu method.[21] The Otsu method is an algorithm to automatically decide the threshold depending on the image using binarization. The mask images were applied to images with the titanium mesh to effectively remove the background and produce phantom-only images. Subsequently, the phantom-only images were divided into the following three section: proximal, area under the titanium mesh; middle, center of the phantom image; distal, area far from the titanium mesh (50 × 150 mm for each area) (Fig. 1d). NAAD was calculated, and the data are presented as median and interquartile range (IQR).

FA dependency in SE and area of excitation dependency in 3D sequences

To confirm FA dependency for RF shielding in SE, FA of 2D SE and 3D TSE was changed to 120° and 150°, respectively. Moreover, to confirm the area of excitation dependency for RF shielding, the number of slices of 3D TSE (FA, 90°) and 3D T_1-FFE was changed to 160 (slice thickness, 1 mm; i.e., the area of excitation, 160 mm). The center of slice (80th slice) was used for analysis. Furthermore, these were compared with the sequence with Table 1 [FA, 90°; slice thickness, 5 mm; the number of slices, 3 (i.e., the area of excitation, 15 mm)] in NAAD of proximal area.

Statistical analysis

The Friedman test, Steel–Dwass multiple comparison test (for NAAD of four sequences in Table 1 and FA dependency in SE), and Wilcoxon signed-rank test (for NAAD of the area of excitation dependency) were used for statistical analyses (EZR Version 1.4.2; Jichi Medical University Saitama Medical Center, Saitama, Japan).[22] A P-value <0.05 was considered statistically significant.

Results

The phantom image is shown in Fig. 2.

Comparison among four T_1-weighted sequences

RF shielding in all sequences was high near the titanium mesh and was low away from the mesh. RF shielding was nearly nonexistent distal to the titanium mesh. The degrees of signal attenuation under the titanium mesh differed depending on the sequences. The signal attenuation ratios near the titanium mesh were 1/5 and 1/3 for 2D SE and 2D TSE, respectively.

As 3D T_1-FFE showed the least RF shielding effect of the titanium mesh, it was deemed the best sequence. The signal attenuation ratio at the position nearest to the titanium mesh for 2D SE was 77.5% larger than that at the position nearest to the titanium mesh for 3D T_1-FFE (Fig. 3a).

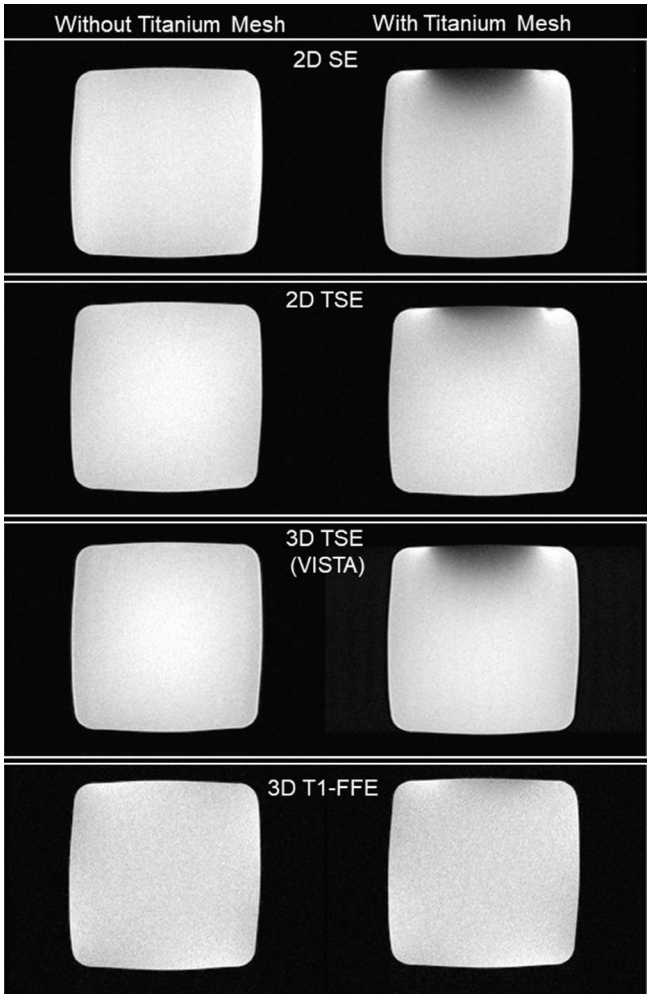

Fig. 2 Phantom image. Combinations without (left) and with the titanium mesh (right) are shown. FFE, fast field echo; SE, spin echo; TSE, turbo spin echo; VISTA, volume isotropic TSE acquisition.

With regard to NAAD, 3D T_1-FFE showed the highest values among the sequences. The median (IQR) NAAD (%) values for 2D SE, 2D TSE, 3D TSE, and 3D T_1-FFE were 71.9 (0.15), 84.7 (1.36), 79.0 (0.05), and 93.9 (1.13), respectively, in the proximal section; 90.3 (0.04), 93.1 (0.18), 90.8 (0.07), and 96.4 (0.09), respectively, in middle section; 90.3 (0.05), 93.4 (0.85), 89.9 (0.02), and 95.3 (0.61), respectively, in distal section. The Friedman test ($P < 0.01$) and Steel–Dwass multiple comparison test ($P < 0.05$) showed significant differences among all combinations (Fig. 3b).

FA dependency in SE and area of excitation dependency in 3D sequences

When FA was increased, RF shielding effect was improved. The median (IQR) NAAD (%) values for FA 90°, 120°, and 150° were 71.9 (0.15), 75.6 (0.07), and 80.1 (0.11), respectively, in 2D SE and 79.0 (0.05), 82.3 (0.08), and 85.5 (0.03), respectively, in 3D TSE. The Friedman test ($P < 0.01$) and Steel–Dwass multiple comparison test ($P < 0.05$) showed significant differences in all combinations (Figs. 4a and 4b). The median (IQR) NAAD (%) values for the area of excitation, 15 and 160 mm, were 79.0 (0.05) and 79.1 (0.03), respectively, in 3D TSE, and 93.9 (1.13) and 91.9 (0.02), respectively, in 3D T_1-FFE. The Wilcoxon signed-rank test showed no significant differences, *P*-value of both sequences was 0.16 (Figs. 4c and 4d).

Discussion

This study does not pursue the physical phenomenon of the RF shielding effect but clarifies the clinical pitfalls of contrast-enhanced MRI examination in patients with a titanium mesh after cranioplasty.

The adopted sequence parameters were based on those in actual frequently used general sequences brain examination with contrast medium (i.e., T_1-weighted sequence). We considered the problem and improvement of the RF shielding effect with regard to clinical relevance in the design of four T_1-weighted sequences.

The RF shielding effect of the titanium mesh on T_1WI was apparent from the signal attenuation ratio and NAAD. RF shielding influenced image uniformity. The B_1 magnetic field and FA were probably decreased by the eddy currents of the changing magnetic field,[6,9] ultimately affecting the echo signal. Thus, the changing magnetic field influenced the images.

In the case of SE (including FSE), even if the frequency shift due to the local magnetic field disturbance is compensated to some extent using the refocused pulse, errors can accumulate because of the time difference between the excitation and refocus pulses in the changed RF, and a suitable compensation effect might not be obtained (e.g., in the lumen of stents).[9] We believe that the same phenomenon occurred near the titanium mesh.

Eddy current time constants in the order of the duration from one RF pulse to another can cause RF shielding during SE imaging.[23] RF shielding had a greater influence on 2D SE than on 2D TSE proximal to the titanium mesh. In FSE (i.e. TSE), even if the refocusing pulse is reduced to <180°, the signal is increased because of the large amount of echo phase refocusing.[24] 2D TSE had three refocusing pulses in this study, whereas SE had only one refocusing pulse. Therefore, we speculate that the increasing signal intensity might be superior to signal reduction by RF shielding effect on 2D TSE. Similarly, 3D TSE (20 refocusing pulses in this study) had the same effect; therefore, the signal intensity was higher than that of 2D SE. However, RF shielding effect by the eddy current in 3D TSE was more influential than that of 2D TSE. We believe that the influence of RF shielding effect could be increased with increasing number of refocusing pulses as compared with increasing signal intensity. This phenomenon depends on the number of refocusing pulses.

Reports have shown that the degradation of image resolution or the extent of the point spread function is caused by

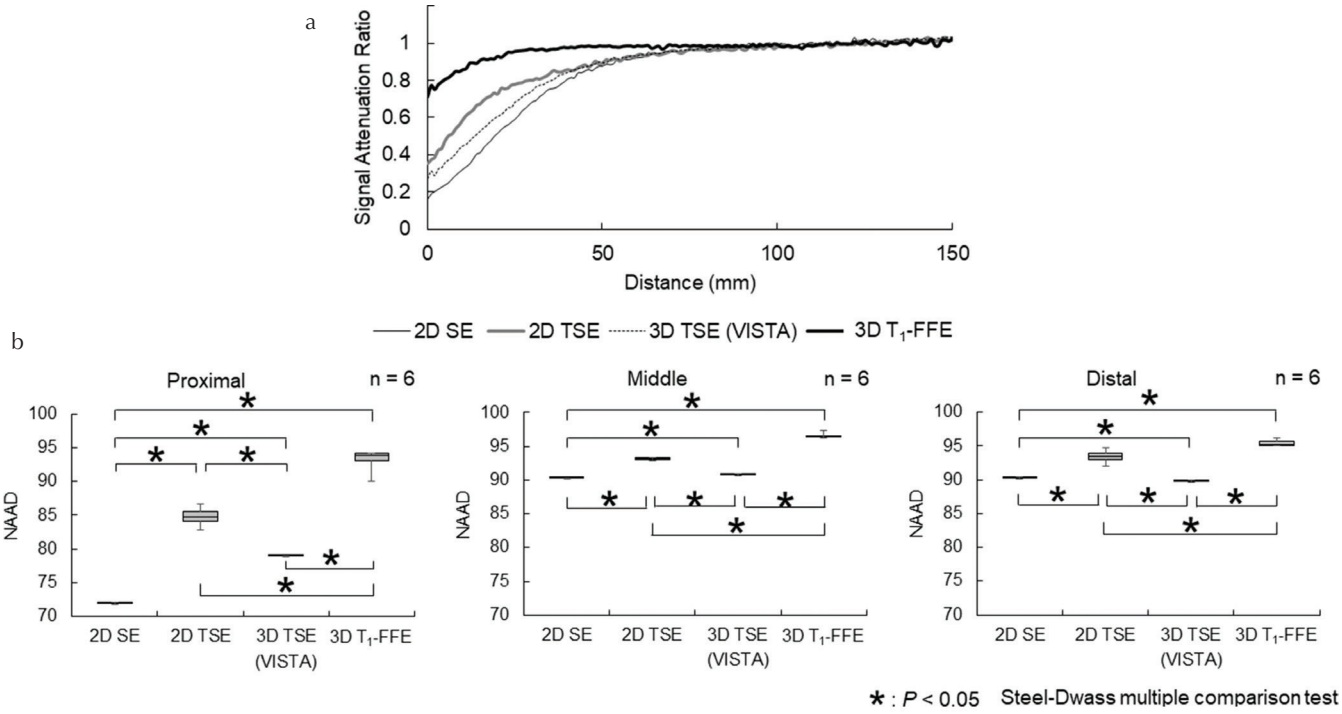

Fig. 3 Comparison among four frequently used general sequences. Signal attenuation ratio (**a**), and NAAD for Proximal, middle, and distal sections of the titanium mesh (**b**). FFE, fast field echo; NAAD, normalized absolute average deviation; SE, spin echo; TSE, turbo spin echo; VISTA, volume isotropic TSE acquisition.

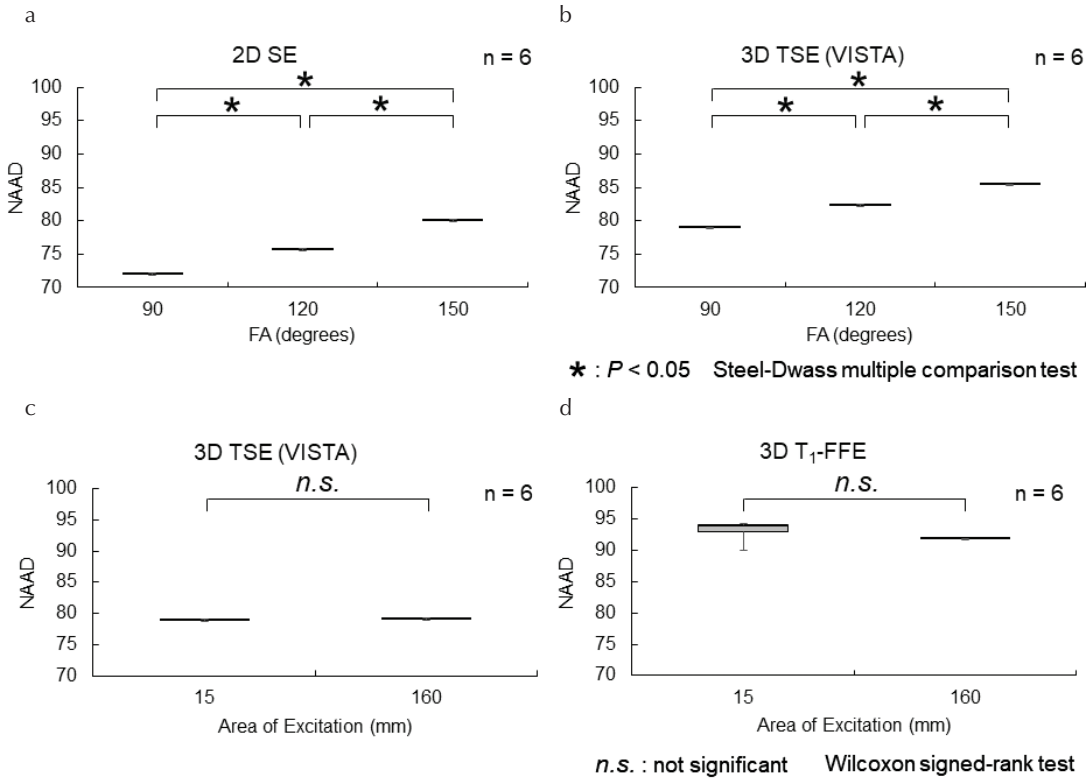

Fig. 4 FA dependency in SE and area of excitation dependency in 3D sequences. The NAAD of FA 90°, 120°, and 150° in 2D SE (**a**) and 3D TSE (VISTA) (**b**), respectively, and the area of excitation for 15 and 160 mm in 3D TSE (VISTA) (**c**) and 3D T_1-FFE (**d**), respectively. FA, flip angle; FFE, fast field echo; NAAD, normalized absolute average deviation; SE, spin echo; TSE, turbo spin echo; VISTA, volume isotropic TSE acquisition.

eddy currents resulting from the time-varying magnetic field during slice selection and frequency encoding.[25] The time-varying magnetic field was different between the SE and GRE sequences.

As the GRE sequence uses an inverse-gradient magnetization field instead of a refocus pulse, there were fewer RF pulses with the GRE sequence than with the SE sequence. When FA for SE was increased, RF shielding was reduced, similar to GRE[8,10]; however, 3D T_1-FFE was less influenced than FA 150° in SE. We considered that the time-varying magnetic field for GRE was less influenced by RF shielding than increased FA for SE. Moreover, when FA was increased for SE, specific absorption ratio also increased; therefore, this aspect should be acknowledged. Hence, the RF shielding effect of 3D T_1-FFE (i.e. GRE) was less influenced and had a higher advantage than SE.

The signal of SE and TSE was lower than that of T_1-FFE (i.e. GRE) in the proximal part of the titanium mesh because the signal acquisition condition was not met owing to the shielding effect of accurate adjustment of the FA.

With regard to the NAAD, 3D T_1-FFE showed the highest values for every combination; hence, uniformity was the highest and the RF shielding effect was the least. Hence, we consider that the RF shielding effect was influenced by the type of sequence.

Although the area of excitation was changed, RF shielding effect would still occur. Therefore, RF shielding effect can occur under any circumstances in the clinical situation.

Figure 5 presents sample images of conventional 2D SE and 3D T_1-FFE with contrast medium obtained in a 46-year-old man 4 years after surgery for a frontal cutaneous fistula and epidural abscess. Similar to this study, a titanium mesh was implanted. The proximal part of the titanium mesh was visualized more clearly with 3D T_1-FFE than with 2D SE.

The 3D GRE sequence could be the most suitable sequence for reducing the RF shielding effect when a patient with a titanium mesh undergoes brain MRI with contrast medium for the identification of remnant tumors and recurrence. Moreover, the advantages of 3D images with an isotropic voxel are high slice resolution and multi-direction through multi-planner reconstruction. Furthermore, small lesions are better visualized with thin 3D sequences.[13,14]

The present study has several limitations. Excitation at the Ernst angle provides the most efficient high signal. However, even if the Ernst angle is known, the signal just proximal to the titanium mesh is excited by a lower energy than that at the set FA owing to the RF shielding effect. Therefore, a sequence involving a high FA could reduce the RF shielding effect in GRE. However, tissue contrast should be considered when FA is modified in a clinical setting.

We considered that a large refocus pulse could be less influenced by RF shielding. This phenomenon is similar to that observed with a FA in that the angle of the refocus pulse is reduced by RF shielding and weaker refocus pulses are affected more greatly. However, the influence of the Ernst angle and refocus pulse were not evaluated. Additionally, the different features of the titanium mesh, such as mesh or hole size,

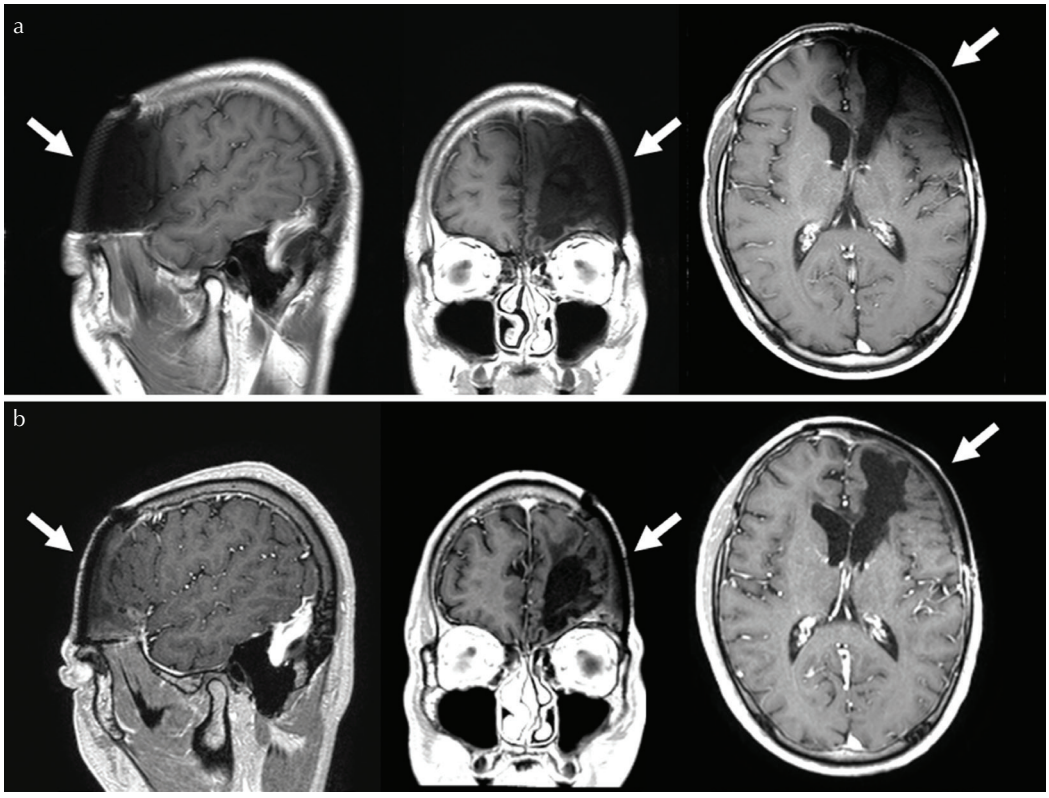

Fig. 5 Sample images of 2D SE (**a**) and 3D T_1-FFE (**b**). Images of a 46-year-old man obtained 4 years after surgery for a frontal cutaneous fistula and epidural abscess with a titanium mesh. The vicinity of the titanium mesh (arrow) is clearer with 3D T_1-FFE than with 2D SE. SE, spin echo; FFE, fast field echo.

thickness, hole interval, and screw for skull fixation, were not assessed, although the influence of stent type on image quality has been reported.[26,27] Moreover, other magnetic strengths were not tested (e.g., 3T). According to a previous report, eddy current effects can be avoided with a long TE.[28] However, the sequences for T_1WI are not suitable or are limited for a long TE owing to the influence of the image weight or contrast.

Although, T_2WI or fluid attenuated inversion recovery should be used to confirm for hematoma and other complications such as superficial brain lesions or cerebral edema after cranioplasty, assessment using these sequences was not performed. Moreover, we surmised that the use of contrast medium would be beneficial after cranioplasty with a titanium mesh; however, the enhancement effect—contrast of the brain region and surrounding tissue—associated with RF shielding was not assessed. Therefore, the use of contrast medium should be further assessed.

Decreases in the transmit RF amplitude (FA decrease) and eddy currents owing to fluctuating RF occur simultaneously, but it is not possible to distinguish which is the more susceptible entity. Furthermore, visual assessment of clinical images with the titanium mesh is required; therefore, additional studies must be performed.

According to our results, when a patient who has undergone cranioplasty with a titanium mesh is subjected to brain MRI, signal attenuation should be considered for the cerebral cortex near the titanium mesh. We consider that 3D GRE could be effective for reducing the RF shielding effect.

Conclusion

3D gradient echo shows the least RF shielding effect of a titanium mesh after cranioplasty among frequently used general sequences for contrast-enhanced brain MRI, and it might be the most appropriate sequence for MRI when a titanium mesh is present.

Acknowledgment

The authors would like to thank Mr. Takuya Komeda in Osaka Red Cross Hospital for his valuable advice and technical support on measurements.

Conflicts of Interest

Yasuo Takatsu received a research grant from the Pfizer Health Research Foundation (2018-2019), and titanium mesh from Bear Medic Corporation. The other authors declare that they have no conflicts of interest.

References

1. Cabraja M, Klein M, Lehmann TN. Long-term results following titanium cranioplasty of large skull defects. Neurosurg Focus 2009; 26:E10.
2. Hill CS, Luoma AM, Wilson SR, Kitchen N. Titanium cranioplasty and the prediction of complications. Br J Neurosurg 2012; 26:832–837.
3. Chiriac A, Stan GE, Iliescu B, Poeata I. The influence of host bone substrate in titanium mesh cranioplasty. Digest J Nanomat Biostruct 2013; 8:729–735.
4. Heredero Jung S, Dean Ferrer A, Solivera Vela J, Alamillos Granados F. Spheno-orbital meningioma resection and reconstruction: the role of piezosurgery and premolded titanium mesh. Craniomaxillofac Trauma Reconstr 2011; 4:193–200.
5. Elephterios B, Dobrin N, Chiriac A. Titanium mesh cranioplasty for patients with large cranial defects. Roman Neurosurg 2010;17:456–460.
6. Takatsu Y, Yamamura K, Miyati T, Kyotani K, Kimura T, Yamatani Y. Radiofrequency-shielding effect of a titanium mesh implanted for cranioplasty. Magn Reson Med Sci 2015; 14:321–327.
7. King KF. Eddy-current Compensation. Chapter 10.3. In: Bernstein MA, King KF, Zhou XJ, eds. Handbook of MRI pulse sequences. London: Elsevier Academic Press, 2004; 316–331.
8. Bartels LW, Bakker CJ, Viergever MA. Improved lumen visualisation in metallic vascular implants by reducing RF artifacts. Magn Reson Med 2002; 47:171–180.
9. Klemm T, Duda S, Machann J, et al. MR imaging in the presence of vascular stents: A systematic assessment of artifacts for various stent orientations, sequence types, and field strengths. J Magn Reson Imaging 2000; 12:606–615.
10. Ikushima Y, Hashido T, Watanabe Y, Doi T. Effects of imaging parameters on the quality of contrast-enhanced MR angiography of cerebral aneurysms treated using stent-assisted coiling: a phantom study. Magn Reson Med Sci 2017; 16:146–151.
11. Kessler AT, Bhatt AA. Brain tumour post-treatment imaging and treatment-related complications. Insights Imaging 2018; 9:1057–1075.
12. Sugahara T, Korogi Y, Ge Y, et al. Contrast enhancement of intracranial lesions: conventional T1-weighted spin-echo versus fast spin-echo MR imaging techniques. AJNR Am J Neuroradiol 1999; 20:1554–1559.
13. Kakeda S, Korogi Y, Hiai Y, et al. Detection of brain metastasis at 3T: comparison among SE, IR-FSE and 3D-GRE sequences. Eur Radiol 2007; 17:2345–2351.
14. Li D, Haacke EM, Tarr RW, Venkatesan R, Lin W, Wielopolski P. Magnetic resonance imaging of the brain with gadopentetate dimeglumine-DTPA: comparison of T1-weighted spin-echo and 3D gradient-echo sequences. J Magn Reson Imaging 1996; 6:415–424.
15. Pui MH, Fok EC. MR imaging of the brain: comparison of gradient-echo and spin-echo pulse sequences. AJR Am J Roentgenol 1995; 165:959–962.
16. Dodo T, Okada T, Yamamoto A, et al. T1-weighted MR imaging of glioma at 3T: a comparative study of 3D MPRAGE vs. conventional 2D spin-echo imaging. Clin Imaging 2016; 40:1257–1261.
17. Suh CH, Jung SC, Kim KW, Pyo J. The detectability of brain metastases using contrast-enhanced spin-echo or gradient-echo images: a systematic review and meta-analysis. J Neurooncol 2016; 129:363–371.

18. Majigsuren M, Abe T, Kageji T, et al. Comparison of brain tumor contrast-enhancement on T1-CUBE and 3D-SPGR images. Magn Reson Med Sci 2016; 15:34–40.
19. National Electrical Manufacturers Association. Determination of Image Uniformity in Diagnostic Magnetic Resonance Images. Rosslyn, VA: NEMA Standards Publication, 2008; 1–17.
20. Takatsu Y, Nakamura M, Yamamura K, et al. A mask method to assess the uniformity of fat suppression in phantom studies. Radiol Phys Technol 2019; 12:417–425.
21. Otsu N. A threshold selection method from gray-level histograms. IEEE Trans Syst Man Cybern 1979; 9:62–66.
22. Kanda Y. Investigation of the freely available easy-to-use software 'EZR' for medical statistics. Bone Marrow Transplant 2013; 48:452–458.
23. Schmitt F. The gradient system. Understanding gradients from an EM perspective: (gradient linearity, eddy currents, maxwell terms & peripheral nerve stimulation). Proc Intl Soc Mag Reson Med 2013; 21:1–13.
24. Hennig J. Multiecho imaging sequences with low refocusing flip angles. J Magn Reson 1988; 78:397–407.
25. De Deene Y, De Wagter C, De Neve W, Achten E. Artefacts in multi-echo T2 imaging for high-precision gel dosimetry: I. Analysis and compensation of eddy currents. Phys Med Biol 2000; 45:1807–1823.
26. Frölich AM, Pilgram-Pastor SM, Psychogios MN, Mohr A, Knauth M. Comparing different MR angiography strategies of carotid stents in a vascular flow model: toward stent-specific recommendations in MR follow-up. Neuroradiology 2011; 53:359–365.
27. Choi JW, Roh HG, Moon WJ, et al. Time-resolved 3D contrast-enhanced MRA on 3.0T: a non-invasive follow-up technique after stent-assisted coil embolization of the intracranial aneurysm. Korean J Radiol 2011; 12:662–670.
28. Frahm J, Merboldt KD, Hänicke W. Localized proton spectroscopy using stimulated echoes. J Magn Reson 1987; 72:502–508.